

Search for associated production of charginos and neutralinos in the trilepton final state using 2.3 fb^{-1} of data

V.M. Abazov³⁶, B. Abbott⁷⁵, M. Abolins⁶⁵, B.S. Acharya²⁹, M. Adams⁵¹, T. Adams⁴⁹, E. Aguilo⁶, M. Ahsan⁵⁹, G.D. Alexeev³⁶, G. Alkhazov⁴⁰, A. Alton^{64,a}, G. Alverson⁶³, G.A. Alves², M. Anastasoae³⁵, L.S. Ancu³⁵, T. Andeen⁵³, B. Andrieu¹⁷, M.S. Anzels⁵³, M. Aoki⁵⁰, Y. Arnoud¹⁴, M. Arov⁶⁰, M. Arthaud¹⁸, A. Askew^{49,b}, B. Åsman⁴¹, A.C.S. Assis Jesus³, O. Atramentov⁴⁹, C. Avila⁸, J. BackusMayes⁸², F. Badaud¹³, L. Bagby⁵⁰, B. Baldin⁵⁰, D.V. Bandurin⁵⁹, P. Banerjee²⁹, S. Banerjee²⁹, E. Barberis⁶³, A.-F. Barfuss¹⁵, P. Bargassa⁸⁰, P. Baringer⁵⁸, J. Barreto², J.F. Bartlett⁵⁰, U. Bassler¹⁸, D. Bauer⁴³, S. Beale⁶, A. Bean⁵⁸, M. Begalli³, M. Biegel⁷³, C. Belanger-Champagne⁴¹, L. Bellantoni⁵⁰, A. Bellavance⁵⁰, J.A. Benitez⁶⁵, S.B. Beri²⁷, G. Bernardi¹⁷, R. Bernhard²³, I. Bertram⁴², M. Besançon¹⁸, R. Beuselinck⁴³, V.A. Bezzubov³⁹, P.C. Bhat⁵⁰, V. Bhatnagar²⁷, G. Blazey⁵², F. Blekman⁴³, S. Blessing⁴⁹, K. Bloom⁶⁷, A. Boehnlein⁵⁰, D. Boline⁶², T.A. Bolton⁵⁹, E.E. Boos³⁸, G. Borissov⁴², T. Bose⁷⁷, A. Brandt⁷⁸, R. Brock⁶⁵, G. Brooijmans⁷⁰, A. Bross⁵⁰, D. Brown¹⁹, X.B. Bu⁷, N.J. Buchanan⁴⁹, D. Buchholz⁵³, M. Buehler⁸¹, V. Buescher²², V. Bunichev³⁸, S. Burdin^{42,c}, T.H. Burnett⁸², C.P. Buszello⁴³, P. Calfayan²⁵, B. Calpas¹⁵, S. Calvet¹⁶, J. Cammin⁷¹, M.A. Carrasco-Lizarraga³³, E. Carrera⁴⁹, W. Carvalho³, B.C.K. Casey⁵⁰, H. Castilla-Valdez³³, S. Chakrabarti⁷², D. Chakraborty⁵², K.M. Chan⁵⁵, A. Chandra⁴⁸, E. Cheu⁴⁵, D.K. Cho⁶², S. Choi³², B. Choudhary²⁸, L. Christofek⁷⁷, T. Christoudias⁴³, S. Cihangir⁵⁰, D. Claes⁶⁷, J. Clutter⁵⁸, M. Cooke⁵⁰, W.E. Cooper⁵⁰, M. Corcoran⁸⁰, F. Couderc¹⁸, M.-C. Cousinou¹⁵, S. Crépe-Renaudin¹⁴, V. Cuplov⁵⁹, D. Cutts⁷⁷, M. Ćwiok³⁰, H. da Motta², A. Das⁴⁵, G. Davies⁴³, K. De⁷⁸, S.J. de Jong³⁵, E. De La Cruz-Burelo³³, C. De Oliveira Martins³, K. DeVaughan⁶⁷, F. Déliot¹⁸, M. Demarteau⁵⁰, R. Demina⁷¹, D. Denisov⁵⁰, S.P. Denisov³⁹, S. Desai⁵⁰, H.T. Diehl⁵⁰, M. Diesburg⁵⁰, A. Dominguez⁶⁷, T. Dorland⁸², A. Dubey²⁸, L.V. Dudko³⁸, L. Duflot¹⁶, S.R. Dugad²⁹, D. Duggan⁴⁹, A. Duperrin¹⁵, S. Dutt²⁷, J. Dyer⁶⁵, A. Dyshkant⁵², M. Eads⁶⁷, D. Edmunds⁶⁵, J. Ellison⁴⁸, V.D. Elvira⁵⁰, Y. Enari⁷⁷, S. Eno⁶¹, P. Ermolov^{38,‡}, M. Escalier¹⁵, H. Evans⁵⁴, A. Evdokimov⁷³, V.N. Evdokimov³⁹, A.V. Ferapontov⁵⁹, T. Ferbel^{61,71}, F. Fiedler²⁴, F. Filthaut³⁵, W. Fisher⁵⁰, H.E. Fisk⁵⁰, M. Fortner⁵², H. Fox⁴², S. Fu⁵⁰, S. Fuess⁵⁰, T. Gadfort⁷⁰, C.F. Galea³⁵, C. Garcia⁷¹, A. Garcia-Bellido⁷¹, V. Gavrilov³⁷, P. Gay¹³, W. Geist¹⁹, W. Geng^{15,65}, C.E. Gerber⁵¹, Y. Gershtein^{49,b}, D. Gillberg⁶, G. Ginther⁷¹, B. Gómez⁸, A. Goussiou⁸², P.D. Grannis⁷², H. Greenlee⁵⁰, Z.D. Greenwood⁶⁰, E.M. Gregores⁴, G. Grenier²⁰, Ph. Gris¹³, J.-F. Grivaz¹⁶, A. Grohsjean²⁵, S. Grünendahl⁵⁰, M.W. Grünewald³⁰, F. Guo⁷², J. Guo⁷², G. Gutierrez⁵⁰, P. Gutierrez⁷⁵, A. Haas⁷⁰, N.J. Hadley⁶¹, P. Haefner²⁵, S. Hagopian⁴⁹, J. Haley⁶⁸, I. Hall⁶⁵, R.E. Hall⁴⁷, L. Han⁷, K. Harder⁴⁴, A. Harel⁷¹, J.M. Hauptman⁵⁷, J. Hays⁴³, T. Hebbeker²¹, D. Hedin⁵², J.G. Hegeman³⁴, A.P. Heinson⁴⁸, U. Heintz⁶², C. Hensel^{22,d}, K. Herner⁷², G. Hesketh⁶³, M.D. Hildreth⁵⁵, R. Hirosky⁸¹, T. Hoang⁴⁹, J.D. Hobbs⁷², B. Hoeneisen¹², M. Hohlfeld²², S. Hossain⁷⁵, P. Houben³⁴, Y. Hu⁷², Z. Hubacek¹⁰, N. Huske¹⁷, V. Hynek⁹, I. Iashvili⁶⁹, R. Illingworth⁵⁰, A.S. Ito⁵⁰, S. Jabeen⁶², M. Jaffré¹⁶, S. Jain⁷⁵, K. Jakobs²³, C. Jarvis⁶¹, R. Jesik⁴³, K. Johns⁴⁵, C. Johnson⁷⁰, M. Johnson⁵⁰, D. Johnston⁶⁷, A. Jonckheere⁵⁰, P. Jonsson⁴³, A. Juste⁵⁰, E. Kajfasz¹⁵, D. Karmanov³⁸, P.A. Kasper⁵⁰, I. Katsanos⁷⁰, V. Kaushik⁷⁸, R. Kehoe⁷⁹, S. Kermiche¹⁵, N. Khalatyan⁵⁰, A. Khanov⁷⁶, A. Kharchilava⁶⁹, Y.N. Kharzheev³⁶, D. Khatidze⁷⁰, T.J. Kim³¹, M.H. Kirby⁵³, M. Kirsch²¹, B. Klima⁵⁰, J.M. Kohli²⁷, J.-P. Konrath²³, A.V. Kozelov³⁹, J. Kraus⁶⁵, T. Kuhl²⁴, A. Kumar⁶⁹, A. Kupco¹¹, T. Kurča²⁰, V.A. Kuzmin³⁸, J. Kvita⁹, F. Lacroix¹³, D. Lam⁵⁵, S. Lammers⁷⁰, G. Landsberg⁷⁷, P. Lebrun²⁰, W.M. Lee⁵⁰, A. Leflat³⁸, J. Lellouch¹⁷, J. Li^{78,‡}, L. Li⁴⁸, Q.Z. Li⁵⁰, S.M. Lietti⁵, J.K. Lim³¹, J.G.R. Lima⁵², D. Lincoln⁵⁰, J. Linnemann⁶⁵, V.V. Lipaev³⁹, R. Lipton⁵⁰, Y. Liu⁷, Z. Liu⁶, A. Lobodenko⁴⁰, M. Lokajicek¹¹, P. Love⁴², H.J. Lubatti⁸², R. Luna-Garcia^{33,e}, A.L. Lyon⁵⁰, A.K.A. Maciel², D. Mackin⁸⁰, R.J. Madaras⁴⁶, P. Mättig²⁶, A. Magerkurth⁶⁴, P.K. Mal⁸², H.B. Malbouisson³, S. Malik⁶⁷, V.L. Malyshev³⁶, Y. Maravin⁵⁹, B. Martin¹⁴, R. McCarthy⁷², M.M. Meijer³⁵, A. Melnitchouk⁶⁶, L. Mendoza⁸, P.G. Mercadante⁵, M. Merkin³⁸, K.W. Merritt⁵⁰, A. Meyer²¹, J. Meyer^{22,d}, J. Mitrevski⁷⁰, R.K. Mommsen⁴⁴, N.K. Mondal²⁹, R.W. Moore⁶, T. Moulik⁵⁸, G.S. Muanza¹⁵, M. Mulhearn⁷⁰, O. Mundal²², L. Mundim³, E. Nagy¹⁵, M. Naimuddin⁵⁰, M. Narain⁷⁷, H.A. Neal⁶⁴, J.P. Negret⁸, P. Neustroev⁴⁰, H. Nilsen²³, H. Nogima³, S.F. Novaes⁵, T. Nunnemann²⁵, D.C. O'Neil⁶, G. Obrant⁴⁰, C. Ochando¹⁶, D. Onoprienko⁵⁹, N. Oshima⁵⁰, N. Osman⁴³, J. Osta⁵⁵, R. Otec¹⁰, G.J. Otero y Garzón¹, M. Owen⁴⁴, M. Padilla⁴⁸, P. Padley⁸⁰, M. Pangilinan⁷⁷, N. Parashar⁵⁶, S.-J. Park^{22,d}, S.K. Park³¹, J. Parsons⁷⁰, R. Partridge⁷⁷, N. Parua⁵⁴, A. Patwa⁷³, G. Pawloski⁸⁰, B. Penning²³, M. Perfilov³⁸, K. Peters⁴⁴, Y. Peters²⁶, P. Pétrouff¹⁶, M. Petteni⁴³, R. Piegaia¹, J. Piper⁶⁵, M.-A. Pleier²²,

P.L.M. Podesta-Lerma^{33,f}, V.M. Podstavkov⁵⁰, Y. Pogorelov⁵⁵, M.-E. Pol², P. Polozov³⁷, B.G. Pope⁶⁵, A.V. Popov³⁹, C. Potter⁶, W.L. Prado da Silva³, H.B. Prosper⁴⁹, S. Protopopescu⁷³, J. Qian⁶⁴, A. Quadt^{22,d}, B. Quinn⁶⁶, A. Rakitine⁴², M.S. Rangel², K. Ranjan²⁸, P.N. Ratoff⁴², P. Renkel⁷⁹, P. Rich⁴⁴, M. Rijssenbeek⁷², I. Ripp-Baudot¹⁹, F. Rizatdinova⁷⁶, S. Robinson⁴³, R.F. Rodrigues³, M. Rominsky⁷⁵, C. Royon¹⁸, P. Rubinov⁵⁰, R. Ruchti⁵⁵, G. Safronov³⁷, G. Sajot¹⁴, A. Sánchez-Hernández³³, M.P. Sanders¹⁷, B. Sanghi⁵⁰, G. Savage⁵⁰, L. Sawyer⁶⁰, T. Scanlon⁴³, D. Schaile²⁵, R.D. Schamberger⁷², Y. Scheglov⁴⁰, H. Schellman⁵³, T. Schliephake²⁶, S. Schlobohm⁸², C. Schwanenberger⁴⁴, R. Schwienhorst⁶⁵, J. Sekaric⁴⁹, H. Severini⁷⁵, E. Shabalina⁵¹, M. Shamim⁵⁹, V. Shary¹⁸, A.A. Shchukin³⁹, R.K. Shivpuri²⁸, V. Siccardi¹⁹, V. Simak¹⁰, V. Sirotenko⁵⁰, P. Skubic⁷⁵, P. Slattery⁷¹, D. Smirnov⁵⁵, G.R. Snow⁶⁷, J. Snow⁷⁴, S. Snyder⁷³, S. Söldner-Rembold⁴⁴, L. Sonnenschein¹⁷, A. Sopczak⁴², M. Sosebee⁷⁸, K. Soustruznik⁹, B. Spurlock⁷⁸, J. Stark¹⁴, V. Stolin³⁷, D.A. Stoyanova³⁹, J. Strandberg⁶⁴, S. Strandberg⁴¹, M.A. Strang⁶⁹, E. Strauss⁷², M. Strauss⁷⁵, R. Ströhmer²⁵, D. Strom⁵³, L. Stutte⁵⁰, S. Sumowidagdo⁴⁹, P. Svoisky³⁵, A. Sznajder³, A. Tanasijczuk¹, W. Taylor⁶, B. Tiller²⁵, F. Tissandier¹³, M. Titov¹⁸, V.V. Tokmenin³⁶, I. Torchiani²³, D. Tsybychev⁷², B. Tuchming¹⁸, C. Tully⁶⁸, P.M. Tuts⁷⁰, R. Unalan⁶⁵, L. Uvarov⁴⁰, S. Uvarov⁴⁰, S. Uzunyan⁵², B. Vachon⁶, P.J. van den Berg³⁴, R. Van Kooten⁵⁴, W.M. van Leeuwen³⁴, N. Varelas⁵¹, E.W. Varnes⁴⁵, I.A. Vasilyev³⁹, P. Verdier²⁰, L.S. Vertogradov³⁶, M. Verzocchi⁵⁰, D. Vilanova¹⁸, F. Villeneuve-Segui⁴³, P. Vint⁴³, P. Vokac¹⁰, M. Voutilainen^{67,g}, R. Wagner⁶⁸, H.D. Wahl⁴⁹, M.H.L.S. Wang⁵⁰, J. Warchol⁵⁵, G. Watts⁸², M. Wayne⁵⁵, G. Weber²⁴, M. Weber^{50,h}, L. Welty-Rieger⁵⁴, A. Wenger^{23,i}, N. Wermes²², M. Wetstein⁶¹, A. White⁷⁸, D. Wicke²⁶, M.R.J. Williams⁴², G.W. Wilson⁵⁸, S.J. Wimpenny⁴⁸, M. Wobisch⁶⁰, D.R. Wood⁶³, T.R. Wyatt⁴⁴, Y. Xie⁷⁷, C. Xu⁶⁴, S. Yacoub⁵³, R. Yamada⁵⁰, W.-C. Yang⁴⁴, T. Yasuda⁵⁰, Y.A. Yatsunenko³⁶, Z. Ye⁵⁰, H. Yin⁷, K. Yip⁷³, H.D. Yoo⁷⁷, S.W. Youn⁵³, J. Yu⁷⁸, C. Zeitnitz²⁶, S. Zelitch⁸¹, T. Zhao⁸², B. Zhou⁶⁴, J. Zhu⁷², M. Zielinski⁷¹, D. Zieminska⁵⁴, L. Zivkovic⁷⁰, V. Zutshi⁵², and E.G. Zverev³⁸

(The $D\bar{0}$ Collaboration)

¹Universidad de Buenos Aires, Buenos Aires, Argentina

²LAFEX, Centro Brasileiro de Pesquisas Físicas, Rio de Janeiro, Brazil

³Universidade do Estado do Rio de Janeiro, Rio de Janeiro, Brazil

⁴Universidade Federal do ABC, Santo André, Brazil

⁵Instituto de Física Teórica, Universidade Estadual Paulista, São Paulo, Brazil

⁶University of Alberta, Edmonton, Alberta, Canada,
Simon Fraser University, Burnaby, British Columbia,
Canada, York University, Toronto, Ontario, Canada,
and McGill University, Montreal, Quebec, Canada

⁷University of Science and Technology of China, Hefei, People's Republic of China

⁸Universidad de los Andes, Bogotá, Colombia

⁹Center for Particle Physics, Charles University, Prague, Czech Republic

¹⁰Czech Technical University, Prague, Czech Republic

¹¹Center for Particle Physics, Institute of Physics,
Academy of Sciences of the Czech Republic, Prague, Czech Republic

¹²Universidad San Francisco de Quito, Quito, Ecuador

¹³LPC, Université Blaise Pascal, CNRS/IN2P3, Clermont, France

¹⁴LPSC, Université Joseph Fourier Grenoble 1, CNRS/IN2P3,
Institut National Polytechnique de Grenoble, Grenoble, France

¹⁵CPPM, Aix-Marseille Université, CNRS/IN2P3, Marseille, France

¹⁶LAL, Université Paris-Sud, IN2P3/CNRS, Orsay, France

¹⁷LPNHE, IN2P3/CNRS, Universités Paris VI and VII, Paris, France

¹⁸CEA, Irfu, SPP, Saclay, France

¹⁹IPHC, Université Louis Pasteur, CNRS/IN2P3, Strasbourg, France

²⁰IPNL, Université Lyon 1, CNRS/IN2P3, Villeurbanne, France and Université de Lyon, Lyon, France

²¹III. Physikalisches Institut A, RWTH Aachen University, Aachen, Germany

²²Physikalisches Institut, Universität Bonn, Bonn, Germany

²³Physikalisches Institut, Universität Freiburg, Freiburg, Germany

²⁴Institut für Physik, Universität Mainz, Mainz, Germany

²⁵Ludwig-Maximilians-Universität München, München, Germany

²⁶Fachbereich Physik, University of Wuppertal, Wuppertal, Germany

²⁷Panjab University, Chandigarh, India

²⁸Delhi University, Delhi, India

²⁹Tata Institute of Fundamental Research, Mumbai, India

³⁰University College Dublin, Dublin, Ireland

- ³¹*Korea Detector Laboratory, Korea University, Seoul, Korea*
³²*SungKyunKwan University, Suwon, Korea*
³³*CINVESTAV, Mexico City, Mexico*
³⁴*FOM-Institute NIKHEF and University of Amsterdam/NIKHEF, Amsterdam, The Netherlands*
³⁵*Radboud University Nijmegen/NIKHEF, Nijmegen, The Netherlands*
³⁶*Joint Institute for Nuclear Research, Dubna, Russia*
³⁷*Institute for Theoretical and Experimental Physics, Moscow, Russia*
³⁸*Moscow State University, Moscow, Russia*
³⁹*Institute for High Energy Physics, Protvino, Russia*
⁴⁰*Petersburg Nuclear Physics Institute, St. Petersburg, Russia*
⁴¹*Lund University, Lund, Sweden, Royal Institute of Technology and Stockholm University, Stockholm, Sweden, and Uppsala University, Uppsala, Sweden*
⁴²*Lancaster University, Lancaster, United Kingdom*
⁴³*Imperial College, London, United Kingdom*
⁴⁴*University of Manchester, Manchester, United Kingdom*
⁴⁵*University of Arizona, Tucson, Arizona 85721, USA*
⁴⁶*Lawrence Berkeley National Laboratory and University of California, Berkeley, California 94720, USA*
⁴⁷*California State University, Fresno, California 93740, USA*
⁴⁸*University of California, Riverside, California 92521, USA*
⁴⁹*Florida State University, Tallahassee, Florida 32306, USA*
⁵⁰*Fermi National Accelerator Laboratory, Batavia, Illinois 60510, USA*
⁵¹*University of Illinois at Chicago, Chicago, Illinois 60607, USA*
⁵²*Northern Illinois University, DeKalb, Illinois 60115, USA*
⁵³*Northwestern University, Evanston, Illinois 60208, USA*
⁵⁴*Indiana University, Bloomington, Indiana 47405, USA*
⁵⁵*University of Notre Dame, Notre Dame, Indiana 46556, USA*
⁵⁶*Purdue University Calumet, Hammond, Indiana 46323, USA*
⁵⁷*Iowa State University, Ames, Iowa 50011, USA*
⁵⁸*University of Kansas, Lawrence, Kansas 66045, USA*
⁵⁹*Kansas State University, Manhattan, Kansas 66506, USA*
⁶⁰*Louisiana Tech University, Ruston, Louisiana 71272, USA*
⁶¹*University of Maryland, College Park, Maryland 20742, USA*
⁶²*Boston University, Boston, Massachusetts 02215, USA*
⁶³*Northeastern University, Boston, Massachusetts 02115, USA*
⁶⁴*University of Michigan, Ann Arbor, Michigan 48109, USA*
⁶⁵*Michigan State University, East Lansing, Michigan 48824, USA*
⁶⁶*University of Mississippi, University, Mississippi 38677, USA*
⁶⁷*University of Nebraska, Lincoln, Nebraska 68588, USA*
⁶⁸*Princeton University, Princeton, New Jersey 08544, USA*
⁶⁹*State University of New York, Buffalo, New York 14260, USA*
⁷⁰*Columbia University, New York, New York 10027, USA*
⁷¹*University of Rochester, Rochester, New York 14627, USA*
⁷²*State University of New York, Stony Brook, New York 11794, USA*
⁷³*Brookhaven National Laboratory, Upton, New York 11973, USA*
⁷⁴*Langston University, Langston, Oklahoma 73050, USA*
⁷⁵*University of Oklahoma, Norman, Oklahoma 73019, USA*
⁷⁶*Oklahoma State University, Stillwater, Oklahoma 74078, USA*
⁷⁷*Brown University, Providence, Rhode Island 02912, USA*
⁷⁸*University of Texas, Arlington, Texas 76019, USA*
⁷⁹*Southern Methodist University, Dallas, Texas 75275, USA*
⁸⁰*Rice University, Houston, Texas 77005, USA*
⁸¹*University of Virginia, Charlottesville, Virginia 22901, USA and*
⁸²*University of Washington, Seattle, Washington 98195, USA*

(Dated: January 6, 2009)

We report the results of a search for associated production of charginos and neutralinos using a data set corresponding to an integrated luminosity of 2.3 fb^{-1} collected with the D0 experiment during Run II of the Tevatron proton-antiproton collider. Final states containing three charged leptons and missing transverse energy are probed for a signal from supersymmetry with four dedicated trilepton event selections. No evidence for a signal is observed, and we set limits on the product of production cross section and leptonic branching fraction. Within minimal supergravity, these limits translate into bounds on m_0 and $m_{1/2}$ that are well beyond existing limits.

PACS numbers: 14.80.Ly, 13.85.Rm, 12.60.Jv

Supersymmetry (SUSY) [1] is one of the most popular extensions of the standard model (SM). SUSY can solve the hierarchy problem, allows the unification of gauge couplings, and provides a dark matter candidate. The analyses presented in this Letter are based on the supersymmetric extension of the SM with minimal field content, the so-called minimal supersymmetric standard model (MSSM), which requires the addition of a SUSY partner for each SM particle, differing by half a unit in spin. The supersymmetric partners of charged and neutral Higgs and gauge bosons form two chargino ($\tilde{\chi}^\pm$) and four neutralino ($\tilde{\chi}^0$) mass eigenstates. Experiments at the CERN e^+e^- Collider (LEP) have set lower limits on the masses of SUSY particles. In particular, charginos with mass lower than 103.5 GeV and sleptons ($\tilde{\ell}$) with mass below 95 GeV are excluded [2]. The results presented here are the extensions of an earlier search for charginos and neutralinos by the D0 collaboration based on 0.3 fb^{-1} of data [3]. The CDF collaboration has published limits for charginos and neutralinos using 2.0 fb^{-1} of data [4].

In $p\bar{p}$ collisions, charginos and neutralinos can be produced in pairs via an off-shell W boson or the exchange of squarks. They decay into fermions and the lightest neutralino $\tilde{\chi}_1^0$, which is assumed to be the lightest supersymmetric particle (LSP) and to escape undetected. This Letter describes the search for $p\bar{p} \rightarrow \tilde{\chi}_1^\pm \tilde{\chi}_2^0$ in purely leptonic decay modes in final states with missing transverse energy \cancel{E}_T and three charged leptons (e, μ or τ). This signature of three leptons can be particularly challenging in regions of parameter space where lepton momenta are very soft due to small mass differences of the SUSY particles. The analyses are based on $p\bar{p}$ collision data at a center-of-mass energy of 1.96 TeV recorded with the D0 detector at the Fermilab Tevatron Collider between March 2002 and June 2007 corresponding to an integrated luminosity of 2.3 fb^{-1} , with the exception of the analysis using identified hadronic τ lepton decays, which is based on 1 fb^{-1} of data.

The D0 detector [5] consists of a central tracking system surrounded by a liquid-argon sampling calorimeter and a muon system. The inner tracking systems, a silicon microstrip tracker and a central fiber tracker, reside in an axial magnetic field of 2 T. The η coverage of the calorimeter extends down to pseudorapidities of $|\eta| \approx 4$, where $\eta = -\ln[\tan(\theta/2)]$ and θ is the polar angle with respect to the proton beam direction. Muons are identified in the inner tracking system as well as in the outer muon system, which consists of three layers of tracking detectors and scintillator counters. An iron toroidal magnet providing a field of 1.8 T is located between the two innermost layers. The muon system provides coverage for muon identification up to $|\eta| \approx 2$. A three-stage real-time trigger system reduces the total rate from 2.5 MHz to about 100 Hz. Events for the offline analyses are collected by a combination of single lepton, di-lepton, and

lepton plus track triggers. Electrons and muons are selected by their specific energy deposition in the calorimeter and hits in the muon chambers, respectively. In addition, high momentum tracks matched to the objects in the calorimeter and muon system help to reduce the trigger rates.

Standard model and SUSY processes are simulated with the event generators PYTHIA [6] (Drell-Yan, diboson, Υ , and $t\bar{t}$ events) and ALPGEN [7] (W +jet/ γ events). The simulation of the detector geometry and response is based on GEANT [8]. Detector noise and additional interactions are included using randomly triggered events recorded throughout the duration of the data-taking period. The predictions for the SM backgrounds are normalized using the next-to-leading (NLO) and, for Drell-Yan production, next-to-NLO theoretical cross sections, calculated using CTEQ6.1M parton distribution functions [9].

The contributions from multijet background are estimated using D0 data. For each analysis, samples dominated by multijet background are defined that are identical to the search samples except for reversed lepton identification requirements. In case of the electrons, jet-like electrons are selected based on the likelihood criterion (see below) while for the muons the isolation criteria (see below) are inverted. The normalization of these samples is performed at an early stage of the selection in a region of phase space that is dominated by multijet production.

The optimization of the analysis is done using minimal supergravity (mSUGRA) [10] as a reference model, in regions of parameter space with chargino, neutralino, and slepton masses ranging from 100 to 200 GeV. The mSUGRA scenario can be described by five independent parameters: the unified scalar and gaugino masses m_0 and $m_{1/2}$, the ratio of the vacuum expectation values of the two Higgs doublets, $\tan\beta$, the unified trilinear coupling A_0 , and the sign of the Higgs mass parameter μ . The SUSY spectra are calculated using SOFTSUSY [11]. The selection criteria are optimized to achieve the best average expected limit under the assumption that no signal is present in the data. A modified frequentist approach [12] is used to calculate limits at the 95% C.L. for each different final state and selection. Two choices of mSUGRA parameters ($m_0 = 150 \text{ GeV}$ and $m_{1/2} = 250$ (170) GeV, with $\tan\beta = 3$, $A_0 = 0$ and $\mu > 0$) are used as a reference for a high- p_T (low- p_T) signal, labeled SUSY1 (SUSY2) in the plots shown in the following.

The reconstruction of isolated electrons exploits their characteristic energy deposition in the calorimeter. All electromagnetic clusters with $|\eta| < 3.2$ are considered. A track is required to point to the calorimeter energy cluster, and the track momentum and the calorimeter energy must be consistent. A likelihood discriminant is used to reject background contributions from jets, based on their differences in transverse and longitudinal shower shape as well as differences in isolation in the tracker. The se-

lection of muons relies on a combination of tracks in the central tracker and pattern of hits in the muon detector within $|\eta| < 2.0$. Isolation criteria are imposed in both the tracker and the calorimeter in order to suppress background contributions from jets. Two different type of muons, referred to as “loose” and “tight”, are used in the analyses. The classification of loose and tight muons depends on the level of calorimeter and tracker isolation of the candidate. The isolation in the calorimeter is based on the cell energies in a hollow cone of $0.1 < \Delta\mathcal{R} < 0.4$, where $\Delta\mathcal{R} = \sqrt{(\Delta\eta)^2 + (\Delta\phi)^2}$. The tracker isolation is defined as the scalar sum of the transverse momenta of all tracks in a cone of $\Delta\mathcal{R} < 0.4$ around the muon track. The energies for both calorimeter and tracker isolation are required to be less than 4 GeV (2.5 GeV) for loose (tight) muons. Reconstruction efficiencies for both e and μ are measured using $Z \rightarrow \ell\ell$ events, and the efficiencies in the Monte Carlo (MC) simulation are corrected for known differences according to the measurements in the data.

The reconstruction of hadronically decaying τ leptons is seeded by calorimeter clusters or tracks [13] with $|\eta| < 2.5$. According to their signature in the detector, they are classified into three types. The signature of τ -type 1 (τ -type 2) consists of a single track with energy deposit in the hadronic (and the electromagnetic) calorimeter typically arising from π^\pm -like (ρ^\pm -like) decays. Three-prong decays (τ -type 3) are not considered here, since the background contribution from jets in this channel does not allow one to improve the sensitivity to a signal. The separation of hadronic τ leptons and jets is based on a set of neural networks (NN), one for each τ -type, exploiting the differences in longitudinal and transverse shower shapes as well as differences in the isolation in the calorimeter and the tracker [13]. $Z \rightarrow \tau\tau$ MC events are used as the signal training sample for the neural networks, while multijet events from data serve as the background training sample. In order to ensure high efficiency for low τ lepton transverse momenta, the selection on the NN output varies depending on the transverse momenta of the τ candidates to keep a constant efficiency of 60%. At a small rate, muons can be misidentified as one-prong hadronic τ lepton decays, and thus τ candidates to which a muon can be matched are rejected.

Jets are reconstructed with an iterative midpoint cone algorithm [14] with cone radius of 0.5 and must be within $|\eta| < 2.5$. The \cancel{E}_T is calculated from the vector sum of the transverse components of the energy deposited in the calorimeter cells and is corrected for electron, τ and jet energy calibrations as well as the transverse momentum of muons.

In the following, four different channels are defined, distinguished by the lepton content of the final state. For the di-electron plus lepton channel ($e\ell$) two identified electrons are required using the electron identification criteria described above. In the di-muon plus lep-

ton channel ($\mu\mu\ell$), one tight and one loose muon are required, while the selection in the electron, muon plus lepton channel ($e\mu\ell$) starts from one electron and one tight muon. Finally, the muon, τ lepton plus lepton channel ($\mu\tau$) requires one tight muon and one hadronically decaying τ lepton in the final state. In all cases, unless explicitly specified otherwise, the third lepton is reconstructed as an isolated track without using the standard lepton identification criteria.

For each of the $e\ell$, $\mu\mu\ell$ and $e\mu\ell$ channels, one “low- p_T ” and one “high- p_T ” selection is designed to exploit the different kinematic properties for various parameter points in the m_0 - $m_{1/2}$ plane. The $\mu\tau$ channel is separated into two distinct selections based on the properties of the third object. One selection requires only an isolated track as third object, as in the other three analyses ($\mu\tau\ell$ selection). For the second selection, a fully reconstructed hadronic τ lepton is required ($\mu\tau\tau$ selection). Both $\mu\tau$ selections are identical over the whole m_0 - $m_{1/2}$ plane.

Each selection requires two identified leptons stemming from the primary vertex with minimum transverse momenta of $p_T^{\ell 1} = 12$ GeV and $p_T^{\ell 2} = 8$ GeV. Due to higher thresholds in the single muon triggers used for the $\mu\tau$ channel, the p_T cut on the muon is tightened to 15 GeV for this channel. If more than two leptons are identified that satisfy the p_T criteria, the two leptons with the highest p_T are considered. In case of the $e\mu\ell$ analysis, events are removed if two electrons or muons with an invariant mass compatible with that of the Z boson mass are found. This is called the preselection. To further reduce the background, differences in the kinematics and event topology compared to signal are exploited. All selection criteria are summarized in Tables I and II.

The dominant background from Drell-Yan and Z boson production in the $\mu\mu\ell$ and $e\ell$ channels as well as multijet background can be reduced by selecting on the invariant mass $m_{\ell_1\ell_2}$ of the identified di-lepton system and the opening angle $\Delta\phi_{\ell_1\ell_2}$ of the same two leptons in the transverse plane. As shown in Fig. 1, a major fraction of the di-lepton events from Z boson decays can be rejected by requiring the invariant mass $m_{\ell_1\ell_2}$ to be below the Z resonance. A substantial fraction of the Drell-Yan events as well as the major part of events from multijet production are back-to-back in the transverse plane and can be rejected by removing events with large opening angle $\Delta\phi_{\ell_1\ell_2}$.

Another striking feature of the signal is the presence of large \cancel{E}_T due to the escaping neutralinos and neutrinos in the final state. Thus selecting events with large \cancel{E}_T is expected to further enhance the signal, which is illustrated in Fig. 2. However, backgrounds without true \cancel{E}_T can potentially satisfy this selection criterion, because of mismeasurements of the objects in the event or by failing to reconstruct them. If \cancel{E}_T is caused by mismeasurement of an object, the direction of the \cancel{E}_T tends to be aligned

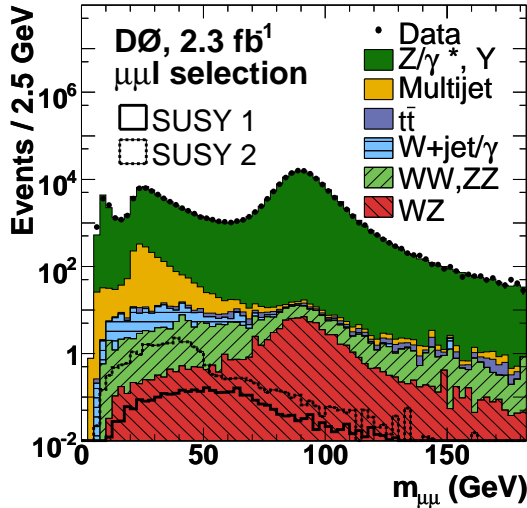


FIG. 1: Invariant mass $m_{\mu\mu}$ ($\mu\mu l$ channel) for data (points), SM backgrounds (shaded histograms), and SUSY signal (open histograms) after cut I (see Table I) for the low- p_T selection.

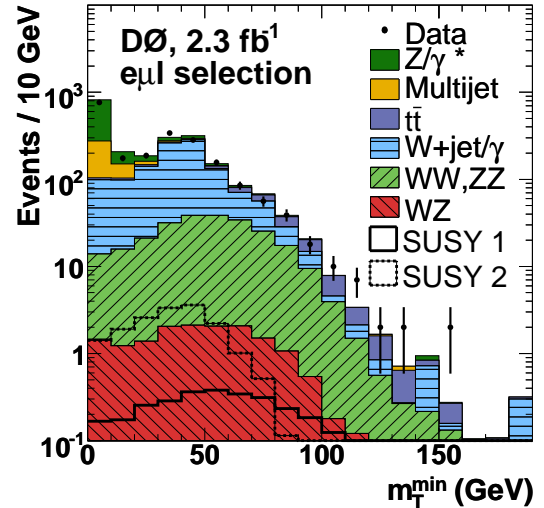


FIG. 3: Minimum transverse mass m_T^{\min} ($e\mu l$ channel) for data (points), SM backgrounds (shaded histograms), and SUSY signal (open histograms) before applying the cut on m_T^{\min} (see Table I) for the low- p_T selection.

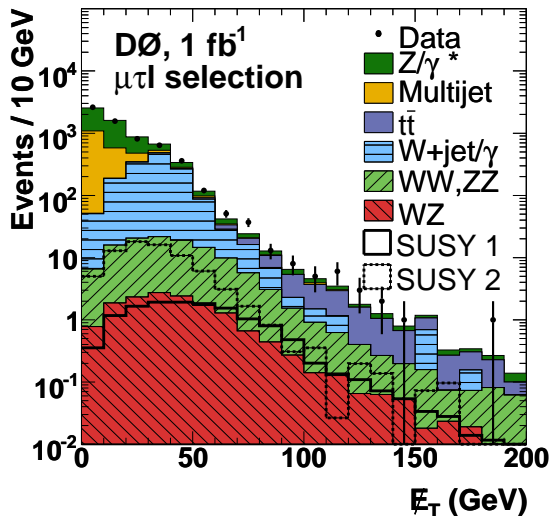


FIG. 2: Missing transverse energy E_T ($\mu\tau l$ selection) for data (points), SM backgrounds (shaded histograms), and SUSY signal (open histograms) after cut I (see Table II).

with this object. For events with at least one jet, $\text{Sig}(E_T)$ is defined as

$$\text{Sig}(E_T) = \frac{E_T}{\sqrt{\sum_{\text{jets}} \sigma^2(E_T^j || E_T)}},$$

where $\sigma(E_T^j || E_T)$ is the jet energy resolution projected on the E_T direction. As a result, $\text{Sig}(E_T)$ is expected to be small for events with poorly measured jets. Rejecting events with small minimal transverse mass $m_T^{\min} = \min(m_T^{\ell_1}, m_T^{\ell_2})$, where $m_T^{\ell} = \sqrt{2p_T^{\ell} E_T [1 - \cos \Delta\phi(\ell, E_T)]}$, removes events with mis-

measured leptons as illustrated in Fig. 3. Other events with large jet activity, in particular $t\bar{t}$ production, can be removed with a cut on H_T , the scalar sum of the p_T of all jets with $p_T > 15$ GeV.

Unlike most SM backgrounds, signal events contain three charged leptons. This can be exploited to remove most of the remaining background, which is dominated by W +jet production at this stage of the selection. The $e\ell l$, $\mu\mu l$, $e\mu l$, and $\mu\tau l$ selections only require an additional track that must be isolated in both the tracking system and the calorimeter as indication of this third lepton. Dropping the lepton identification criteria in this case increases the signal efficiency and includes all three lepton flavors in the selection. The distribution of the transverse momentum of this additional track is presented in Fig. 4 after E_T , $\text{Sig}(E_T)$ and m_T^{\min} cuts are applied. Selection of tracks with high transverse momentum clearly enhances signal over background. For the $\mu\tau\tau$ channel, a well-identified second τ lepton is required instead of the track. Since the τ lepton selection imposes different criteria than the track selection, some signal loss due to the third track criterion can be regained using this selection. In particular at high $\tan\beta$, this selection is favored, since most of the leptons in the final state are expected to be τ leptons. Figure 5 shows the distribution of the transverse momentum for the second τ lepton candidate.

After the third object selection, the remaining background consists mainly of W and Z boson as well as di-boson production. These backgrounds are addressed in the following. The remaining Z boson background mainly consists of events where one of the leptons from the Z boson decay is not reconstructed in the calorime-

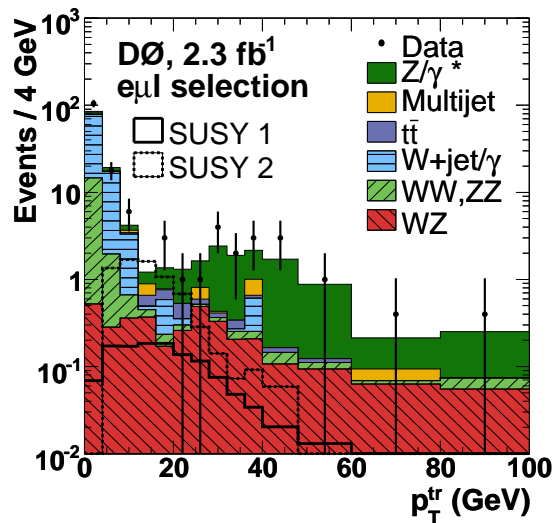


FIG. 4: Transverse momentum of the track ($e\mu l$ channel) for data (points), SM backgrounds (shaded histograms), and SUSY signal (open histograms) after all \cancel{E}_T related cuts are applied (cut III, see Table I) for the low- p_T selection.

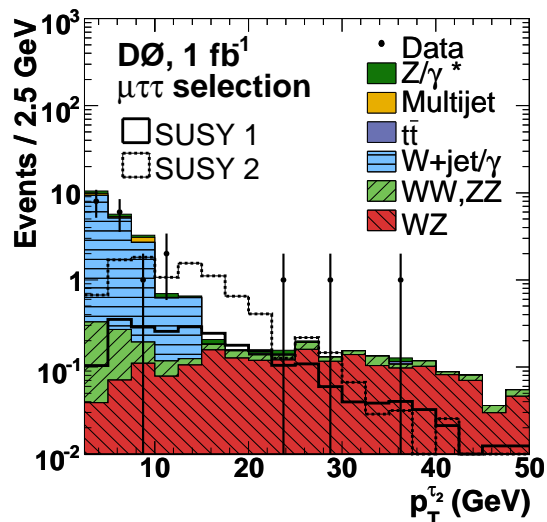


FIG. 5: Transverse momentum of the second τ lepton candidate ($\mu\tau\tau$ selection) for data (points), SM backgrounds (shaded histograms), and SUSY signal (open histograms) after cut III (see Table II).

ter or muon system, but instead a jet or photon from initial or final state radiation is misidentified as one of the two initially selected leptons. However, the missed lepton from the Z boson decay is then selected as the third track. This unique feature provides two handles to reject this background. Due to the non-reconstruction of one of the leptons, the \cancel{E}_T tends to point into the direction of the track. Thus the transverse mass calculated from the track and \cancel{E}_T should be small due to the small opening angle $\Delta\phi_{tr,\cancel{E}_T}$. In addition, the invariant mass of

the track and one of the leptons, $m_{\ell_{1,2},tr}$, is expected to be consistent with the Z boson mass. The same is true for WZ production, where again one of the leptons from the Z decay is reconstructed in the tracking system.

For W boson production, only one real lepton is expected from the decay of the W boson, the second lepton is mimicked by a jet or a photon. In the case of jets, the identification criteria for that lepton tend to be of worse quality, while in case of photon conversions, no hits in the innermost layers of the tracking detector are expected for the track corresponding to the converted photon. Thus, requiring high quality leptons (tight likelihood for electrons and very tight track isolation for muons) or hits in the first two layers of the tracking system is expected to reduce $W+\text{jet}/\gamma$ background. To keep signal efficiencies high, these requirements are only used if the event properties and kinematics are similar to expectations from W boson production (see Table I). In case of the $\mu\tau l$ selection, a dedicated likelihood discriminant is developed to remove the background from W boson production. This likelihood uses the transverse masses calculated for all of the three leptons as well as products of \cancel{E}_T and lepton transverse momenta. In case of the $\mu\tau\tau$ selection, the product of the two NN outputs for τ lepton identification is used to remove events containing misidentified τ candidates.

Finally, the different event kinematics for signal and background are exploited to obtain better signal sensitivity. Since background is expected to have low transverse momentum for the third track or small \cancel{E}_T , a cut on the product of track p_T and \cancel{E}_T effectively rejects any remaining background contributions. In addition, the vectorial sum of the lepton transverse momenta and \cancel{E}_T should equal the transverse momentum of the third track in case of signal events. Thus the p_T balance

$$p_T^{\text{bal}} = \frac{|\vec{p}_T^{\ell_1} + \vec{p}_T^{\ell_2} + \vec{\cancel{E}}_T|}{p_T^{\text{tr}}}$$

is expected to peak at 1 for a signal, while for background a broad distribution is expected.

After all selection criteria are applied, the expected background is dominated by irreducible background from WZ production, as is evident from the marginal distribution of the di-electron invariant mass in the eel selection shown in Fig. 6. A detailed comparison of background expectation and events observed in data together with efficiency expectations from a typical SUSY signal are shown in Tables III and IV for the low- p_T and high- p_T selection, respectively, while Table V presents the results for the $\mu\tau$ selections. In general, good agreement between data and expectation from SM processes is observed. Combining all low- p_T and $\mu\tau$ selections, a background of $5.4 \pm 0.4(\text{stat}) \pm 0.4(\text{syst})$ events from SM processes is expected with 9 events observed in the data. The probability to observe 9 or more events in the data given the expected

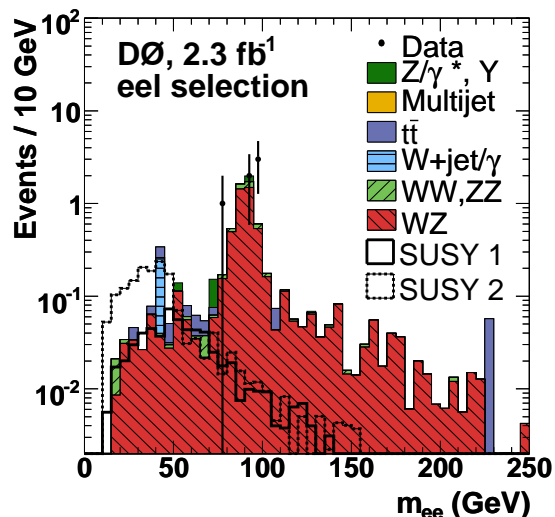


FIG. 6: Distribution of the invariant mass m_{ee} (eel channel) for data (points), SM backgrounds (shaded histograms), and SUSY signal (open histograms) with all cuts applied except the m_{ee} requirement for the low- p_T selection.

background is 10%. The expectation for the reference signal point SUSY2 is $9.3 \pm 0.3(\text{stat}) \pm 0.8(\text{syst})$ events. The high- p_T selection yields $3.3 \pm 0.3(\text{stat}) \pm 0.3(\text{syst})$ events from SM processes, while 4 events are observed in data. The expected reference signal for parameter point SUSY1 is $0.9 \pm 0.1(\text{stat}) \pm 0.1(\text{syst})$ events.

The estimate of the expected numbers of signal and background events depends on various measurements with associated systematic uncertainties: integrated luminosity (6%) [15], trigger efficiency, lepton identification and reconstruction efficiencies (4%), jet and τ energy calibration in signal (2%–6%) and background events (2%–9%), PDF uncertainties (3%–4%), and modeling of the multijet background (2%–30%). All uncertainties, except the last one, are correlated among the different channels.

No evidence for a signal is observed. The search results can be translated into upper limits on the product of cross section and branching fraction into three charged leptons, $\sigma \times \text{BR}(3\ell)$. Limits are based on the combination of all low- and high- p_T selections. Events appearing in multiple analyses are uniquely assigned to the channel with the best signal to background ratio. Correlated systematic uncertainties are taken into account.

To calculate the limits, the mass relations between the particles involved in the decay chain of chargino and neutralino have to be known. The mSUGRA model is used to calculate the mass differences between $\tilde{\chi}_1^\pm$, $\tilde{\chi}_2^0$, and $\tilde{\chi}_1^0$, which approximately corresponds to the assumption $m_{\tilde{\chi}_1^\pm} \approx m_{\tilde{\chi}_2^0} \approx 2m_{\tilde{\chi}_1^0}$. For slepton and sneutrino masses, several scenarios are taken into account.

Figure 7 shows the limit on $\sigma \times \text{BR}(3\ell)$ as a function of chargino mass assuming that sleptons and sneutrinos are heavier than the lightest chargino and the second-lightest

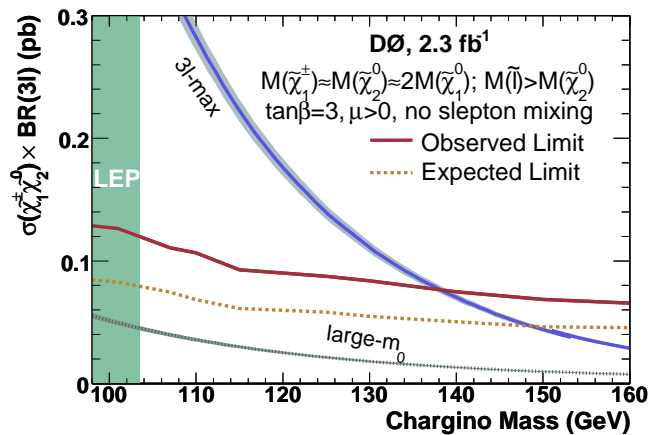


FIG. 7: Upper limit at the 95% C.L. on $\sigma \times \text{BR}(3\ell)$ as a function of $\tilde{\chi}_1^\pm$ mass, in comparison with the expectation for two SUSY scenarios (see text). PDF and renormalization/factorization scale uncertainties on the predicted cross section are shown as shaded bands.

neutralino, and assuming that slepton mixing can be neglected. In this case, both $\tilde{\chi}_1^\pm$ and $\tilde{\chi}_2^0$ decay via three-body decays, and branching fractions do not depend on the lepton flavor. The limit is compared with the NLO cross section [16] multiplied by branching fractions calculated in the limit of heavy sleptons (“large- m_0 ” scenario) and for slepton masses just above the mass of the $\tilde{\chi}_2^0$, in which case the leptonic branching fraction for three-body decays is maximized (“3l-max” scenario). For the latter, an observed (expected) lower limit at the 95% C.L. on the chargino mass is set at 138 GeV (148 GeV).

Alternatively, the results can be interpreted within mSUGRA. To obtain the efficiency for any given point in the m_0 – $m_{1/2}$ plane, selection efficiencies are first determined separately for three-body decays of chargino and neutralino as well as two-body decays via sleptons and sneutrinos. The variation of these efficiencies throughout the plane can then be parametrized for each selection as a function of the chargino, slepton and sneutrino masses. Using the mSUGRA prediction of branching fractions and masses [6] [11] [17], the parametrized efficiencies are used to calculate the total efficiency for each point in the m_0 – $m_{1/2}$ plane. Figure 8 shows the region excluded in the m_0 – $m_{1/2}$ plane for $\tan\beta = 3$, $A_0 = 0$ and $\mu > 0$ in comparison with the limits from chargino and slepton searches at LEP [2] and CDF [4]. The shape of the excluded region is driven by the relation of gaugino and slepton masses throughout the plane, which affects the branching fraction into three charged leptons as well as the efficiencies of the selections. For slepton masses just below the $\tilde{\chi}_2^0$ mass, one of the leptons from the $\tilde{\chi}_2^0$ decay has very small momentum, rendering the tripleton selections inefficient. For sneutrinos lighter than the $\tilde{\chi}_1^\pm$ and $\tilde{\chi}_2^0$, two-body decays into sneutrinos open up, leading to a smaller branching fraction into three charged leptons

TABLE I: Selection criteria for the $\mu\mu\ell$, eel and $e\mu\ell$ analyses (all energies, masses and momenta in GeV, angles in radians) for the low- p_T selection and high- p_T selection, see text for further details.

Selection	$\mu\mu\ell$		eel		$e\mu\ell$		
	low p_T	high p_T	low p_T	high p_T	low p_T	high p_T	
I	$p_T^{\ell_1}, p_T^{\ell_2}$	>12, >8	>18, >16	>12, >8	>20, >10	>12, >8 ^a	>15, >15
	$m_{\ell_1\ell_2}$ ^b	$\in [20, 60]$	$\in [0, 75]$	$\in [18, 60]$	$\in [0, 75]$	–	–
II	$\Delta\phi_{\ell_1\ell_2}$	<2.9	<2.9	<2.9	<2.9	–	–
	\cancel{E}_T	>20	>20	>22	>20	>20	>20
	Sig(\cancel{E}_T)	>8	>8	>8	>8	>8	>8
	m_T^{\min}	>20	>20	>20	>14	>20	>15
III	jet-veto H_T	–	<80	–	–	–	–
IV	p_T^{tr}	>5	>4	>4	>12	>6	>6
	m_T^{tr}	>10	>10	>10	>10	>10	>8
V	$m_{\ell_{1,2},tr}$	$\notin [80, 110]$	–	–	–	<70	<70
VI	anti W	–	–	tight likelihood ^c	–	tight likelihood ^d hit in 2 inner layers ^d very tight muon isolation ^e $\sum_{0.05 < \Delta\mathcal{R} < 0.4} p_T^{\text{track}} < 1$	–
	$\cancel{E}_T \times p_T^{tr}$	>200	>300	>220	–	–	–
VII	p_T^{bal}	<4	<4	<4	<4	<2	<2

^a $p_T^{\ell_1}$ and $p_T^{\ell_2}$ are electron and muon p_T , respectively.

^b ℓ refers to the two identified leptons

^cfor $p_T^{tr} < 15$ GeV

^dfor $m_T^{\mu} \in [40, 90]$ GeV

^efor $m_T^e \in [40, 90]$ GeV

TABLE II: Criteria for the $\mu\tau\ell$ and $\mu\tau\tau$ selections (all energies, masses and momenta in GeV, angles in radians), see text for further details.

Selection	$\mu\tau\ell$	$\mu\tau\tau$		
I	$p_T^{\ell_1}, p_T^{\ell_2}$	>15, >8 ^a		
II	$\Delta\phi_{\ell_1\ell_2}$	<2.9		
	\cancel{E}_T	>20		
	Sig(\cancel{E}_T)	>8		
	m_T^{μ}	>20		
III	jet-veto H_T	<80		
IV	p_T^{tr}	$p_T^{\tau_2}$	>4	
	$\Delta\phi_{tr,\cancel{E}_T}$	$\Delta\phi_{\tau_2,\cancel{E}_T}$	>0.5	
V	$m_{\ell_{1,2},tr}$	<60	<60	
	anti W	likelihood	likelihood	
VI		$NN_{\tau_1} \times NN_{\tau_2}$	>0.7	
VII	$\cancel{E}_T \times p_T^{tr}$	>300	p_T^{bal}	<3.5

^a $p_T^{\ell_1}$ and $p_T^{\ell_2}$ are muon and τ lepton p_T , respectively.

as well as a reduced selection efficiency due to the small mass difference between sneutrino and chargino. For the intermediate region at $m_{1/2} \approx 245$ GeV, chargino decays via W bosons compete with decays via sleptons, leading to a reduction in leptonic branching fraction with increasing $m_{1/2}$ both below and above the threshold for

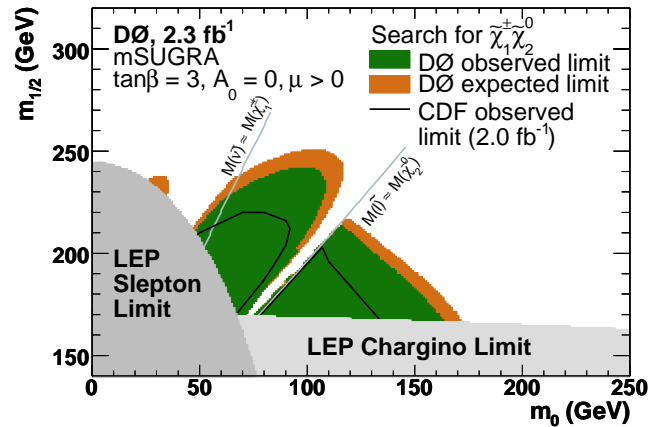


FIG. 8: Region in the m_0 - $m_{1/2}$ plane excluded by the combination of the D0 analyses (green), by LEP searches for charginos (light grey) and sleptons (dark grey) [2] and CDF (black line) [4]. The assumed mSUGRA parameters are $\tan\beta = 3$, $A_0 = 0$ and $\mu > 0$.

production of a real W boson.

The excluded region in the m_0 - $m_{1/2}$ plane depends on the choice of $\tan\beta$, as the branching fraction into τ leptons increases as a function of $\tan\beta$. Figure 9 shows the limit on $\sigma \times \text{BR}(3\ell)$ as a function of $\tan\beta$ for a chargino mass of 130 GeV and fixing m_0 such that the lightest stau

TABLE III: Numbers of events observed in data and expected for background and reference signal efficiency (SUSY2, see text) in percent at various stages of the selection with statistical uncertainties for the low- p_T selection. Each row corresponds to a group of cuts, as detailed in Table I.

Selection	$\mu\mu\ell$			eel			$e\mu\ell$		
	Data	Backgrd.	Eff. (%)	Data	Backgrd.	Eff. (%)	Data	Backgrd.	Eff. (%)
I	194006	195557 \pm 177	19.9 \pm 0.3	235474	232736 \pm 202	15.5 \pm 0.2	16630	16884 \pm 75	10.5 \pm 0.1
II	22766	26067 \pm 88	14.6 \pm 0.2	31365	27184 \pm 64	11.0 \pm 0.2			
III	178	181 \pm 6.4	8.8 \pm 0.1	515	512 \pm 12	6.8 \pm 0.2	1191	1177 \pm 20	5.8 \pm 0.1
IV	7	2.9 \pm 0.7	3.4 \pm 0.1	16	9.3 \pm 2.0	3.0 \pm 0.1	22	18.0 \pm 1.2	2.4 \pm 0.1
V	4	2.2 \pm 0.5	3.0 \pm 0.1	9	5.9 \pm 1.7	2.5 \pm 0.1	3	3.5 \pm 0.5	2.0 \pm 0.1
VI				6	3.1 \pm 0.4	2.2 \pm 0.1	2	1.6 \pm 0.4	1.5 \pm 0.1
VII	4	1.2 \pm 0.2	2.8 \pm 0.1	2	1.8 \pm 0.2	2.1 \pm 0.1	2	0.8 \pm 0.2	1.3 \pm 0.1

TABLE IV: Numbers of events observed in data and expected for background and reference signal efficiency (SUSY1, see text) in percent at various stages of the selection with statistical uncertainties for the high- p_T selection. Each row corresponds to a group of cuts, as detailed in Table I.

Selection	$\mu\mu\ell$			eel			$e\mu\ell$		
	Data	Backgrd.	Eff. (%)	Data	Backgrd.	Eff. (%)	Data	Backgrd.	Eff. (%)
I	140417	141781 \pm 120	19.6 \pm 0.2	171001	170197 \pm 175	18.1 \pm 0.2	4617	4709 \pm 23	11.5 \pm 0.2
II	10349	10645 \pm 51	15.3 \pm 0.2	8273	7937 \pm 39	12.8 \pm 0.1			
III	173	176 \pm 5.7	11.4 \pm 0.2	244	264 \pm 10	10.8 \pm 0.1	727	738 \pm 11	8.9 \pm 0.1
IV	7	3.8 \pm 0.5	5.9 \pm 0.1	0	1.5 \pm 0.3	4.0 \pm 0.1	11	12.7 \pm 0.9	4.1 \pm 0.1
V	4	2.9 \pm 0.4	5.5 \pm 0.1	0	1.1 \pm 0.3	3.6 \pm 0.1	2	2.8 \pm 0.5	2.9 \pm 0.1
VI							0	1.0 \pm 0.2	2.4 \pm 0.1
VII	4	2.0 \pm 0.3	5.0 \pm 0.1	0	0.8 \pm 0.1	3.6 \pm 0.1	0	0.5 \pm 0.1	2.1 \pm 0.1

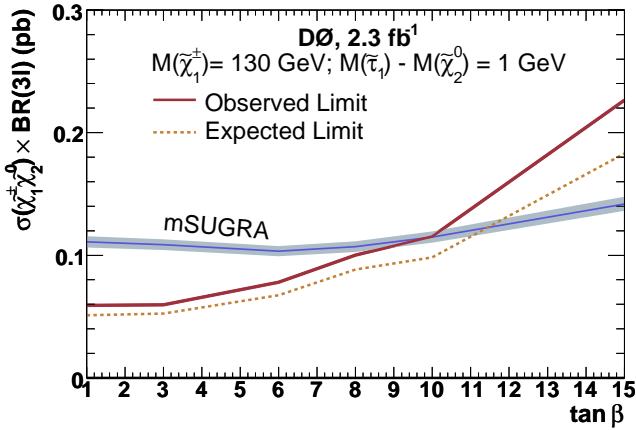


FIG. 9: Upper limit at the 95% C.L. on $\sigma \times \text{BR}(3\ell)$ as a function of $\tan\beta$ in comparison with the prediction for a chargino mass of 130 GeV and $m_{\tilde{\tau}} - m_{\tilde{\chi}_2^0} = 1$ GeV.

($\tilde{\tau}_1$) is heavier than the $\tilde{\chi}_2^0$ by 1 GeV. The latter choice results in three-body decays with maximal leptonic branching fraction. The leptonic branching fraction into three τ leptons increases as a function of $\tan\beta$, reaching values above 50% for $\tan\beta > 15$. Because all selections have been designed to be efficient for τ leptons, the limit remains stable within a factor of two for $\tan\beta \lesssim 10$, allowing one to exclude charginos with a mass of 130 GeV up to $\tan\beta$ of 9.6.

To summarize, a data set collected with the D0 detector corresponding to an integrated luminosity of 2.3 fb $^{-1}$ has been analyzed in search of the associated production of charginos and neutralinos in final states with three charged leptons and \cancel{E}_T . No evidence for a signal is observed, and upper limits on the product of production cross section and leptonic branching fraction have been set. Within the reference model of mSUGRA with $\tan\beta = 3$, $A_0 = 0$, and $\mu > 0$, this result translates into excluded regions in the m_0 - $m_{1/2}$ plane that significantly extend beyond all existing limits from direct searches for supersymmetric particles.

We thank the staffs at Fermilab and collaborating institutions, and acknowledge support from the DOE and NSF (USA); CEA and CNRS/IN2P3 (France); FASI, Rosatom and RFBR (Russia); CNPq, FAPERJ, FAPESP and FUNDUNESP (Brazil); DAE and DST (India); Colciencias (Colombia); CONACyT (Mexico); KRF and KOSEF (Korea); CONICET and UBACyT (Argentina); FOM (The Netherlands); STFC (United Kingdom); MSMT and GACR (Czech Republic); CRC Program, CFI, NSERC and WestGrid Project (Canada); BMBF and DFG (Germany); SFI (Ireland); The Swedish Research Council (Sweden); CAS and CNSF (China); and the Alexander von Humboldt Foundation (Germany).

TABLE V: Numbers of events observed in data and expected for background and reference signal efficiency (SUSY2 for the $\mu\tau\ell$ selection and SUSY1 for the $\mu\tau\tau$ selection, see text) in percent at various stages of the selection with statistical uncertainties for the $\mu\tau$ selections. Each row corresponds to a group of cuts, as detailed in Table II.

Selection	$\mu\tau\ell$			$\mu\tau\tau$		
	Data	Backgrd.	Eff. (%)	Data	Backgrd.	Eff. (%)
I	6251	6238 ± 30	8.1 ± 0.2	6251	6238 ± 30	12.4 ± 0.2
II	3473	3416 ± 17	6.9 ± 0.2	3473	3416 ± 17	10.8 ± 0.2
III	1180	1154 ± 14	4.5 ± 0.1	1180	1154 ± 14	8.7 ± 0.1
IV	103	110.0 ± 5.1	2.9 ± 0.1	20	22.6 ± 2.6	2.2 ± 0.1
V	67	52.8 ± 4.1	2.1 ± 0.1	7	8.0 ± 1.5	1.7 ± 0.1
VI	4	2.9 ± 0.4	1.5 ± 0.1	3	1.9 ± 0.5	1.4 ± 0.1
VII	0	0.8 ± 0.1	1.2 ± 0.1	1	0.8 ± 0.2	1.3 ± 0.1

- [a] Visitor from Augustana College, Sioux Falls, SD, USA.
[b] Visitor from Rutgers University, Piscataway, NJ, USA.
[c] Visitor from The University of Liverpool, Liverpool, UK.
[d] Visitor from II. Physikalisches Institut, Georg-August-University, Göttingen, Germany.
[e] Visitor from Centro de Investigacion en Computacion - IPN, Mexico City, Mexico.
[f] Visitor from ECFM, Universidad Autonoma de Sinaloa, Culiacán, Mexico.
[g] Visitor from Helsinki Institute of Physics, Helsinki, Finland.
[h] Visitor from Universität Bern, Bern, Switzerland.
[i] Visitor from Universität Zürich, Zürich, Switzerland.
[†] Deceased.
- [1] H.E. Haber and G.L. Kane, Phys. Rep. **117**, 75 (1985).
[2] LEPSUSYWG, ALEPH, DELPHI, L3 and OPAL Collaborations, notes LEPSUSYWG/01-03.1 and 04-01.1 (<http://lepsusy.web.cern.ch/lepsusy/Welcme.html>).
[3] V.M. Abazov *et al.* (D0 Collaboration), Phys. Rev. Lett. **95**, 151805 (2005).

- [4] T. Aaltonen *et al.* (CDF Collaboration), Phys. Rev. Lett. **101**, 251801 (2008).
[5] V.M. Abazov *et al.* (D0 Collaboration), Nucl. Instrum. Methods Phys. Res. A **565**, 463 (2006).
[6] T. Sjöstrand *et al.*, Comput. Phys. Commun. **135**, 238 (2001).
[7] M.L. Mangano *et al.*, JHEP **07**, 001 (2003).
[8] R. Brun and F. Carminati, CERN Program Library Long Writeup W5013, 1993 (unpublished).
[9] J. Pumplin *et al.*, JHEP **0207**, 012 (2002); D. Stump *et al.*, JHEP **0310**, 046 (2003).
[10] H.P. Nilles, Phys. Rep. **110**, 1 (1984).
[11] B.C. Allanach, Comput. Phys. Commun. **143**, 305 (2002).
[12] T. Junk, Nucl. Instrum. Methods A **434**, 435 (1999).
[13] V.M. Abazov *et al.* (D0 Collaboration), Phys. Lett. B **670** 292-299 (2009).
[14] G.C. Blazey *et al.*, arXiv:hep-ex/0005012 (2000).
[15] T. Andeen *et al.*, FERMILAB-TM-2365 (2007).
[16] W. Beenakker *et al.*, Phys. Rev. Lett. **83**, 3780 (1999), [Erratum-ibid. **100**, 029901 (2008)].
[17] M. Mühlleitner, A. Djouadi, Y. Mambrini, Comput. Phys. Commun. **168**, 46 (2005).